DOI: 10.63550/ICEIP.2025.71.65.051

Torque of a Two-Tier Wind Turbine Rotor and its Aerodynamic Features

Ulugbek Gofurovich Dekhkonov[1][a], Utkir Gulyamovich Urishev [1][b] and Insomiddin Biloldinovich Najmiddinov [1][c], Shaxlo Tagayevna Ulasheva[2][d]
[1]*Namangan State Technical University, Islam Karimov Street, Namangan, Uzbekistan*
[2]*Karshi State Technical University, Mustaqillik Street, Karshi, Uzbekistan*
urisheva80@mail.ru

Keywords: two-tier rotor, wind turbine, aerodynamic characteristics, driving torque, opposite rotation, open-center blade design.

Abstract: This paper investigates the aerodynamic features and torque characteristics of a novel two-tier wind turbine rotor with counter-rotating blades and an open-center wing design. The structure enhances airflow and energy conversion efficiency by allowing static air suction behind the blades. Mathematical models describe the dynamic interaction between rotor tiers, accounting for pressure differentials and angular motion. The proposed rotor design, adaptable to variable wind directions, demonstrates improved thrust coefficients and mechanical stability. Analytical expressions for torque are derived for different blade positions, enabling precision in simulation. This innovative concept enhances wind energy utilization with the simplicity of three-blade efficiency and six-blade output.

1 INTRODUCTION

Based on the results of the conducted scientific research, we come to the following conclusions in order to design an effective, independent wind direction vector, large-diameter, small-speed and high-power wind turbine rotor construction suitable for the wind regions of our Republic and our technological capabilities (Manwell, 2009; Zhang, 2023; Chaurasiya, 2019).

The bottom line is that a rotor producing 6 blades of energy must have the useful efficiency of a 3-blade rotor. Also, the aerodynamic properties of the rotor should be high, i.e., the process of passive air absorption behind the wing should be accelerated and the coefficient of resistance of the nose should be increased, so that the wind flow can be quickly moved away from the rotor by transferring its kinetic energy (Jain, 2010; Dekhkanov, 2024).

Let the height of the prototype rotor be h m (Fig. 1). We divide it into two equal parts with a horizontal plane P at a height of *h*/2 m. We turn its separated second - upper tier part 1800 around the *X* axis in the counterclockwise direction. A top view of both of their parts is shown in Figures 2a and 2b. It can be seen from them (Figure 1 shows a 4-bladed rotor) that the proposed design is considered in the case of a 3-bladed rotor. It can be seen that the rotor layer shown in Fig. 2a moves counterclockwise, and the rotor layer shown in Fig. 2b moves clockwise: the active vane 2 of the shaft 1 moves under the wind pressure received by the closed plates 3, vanes 4 and 5 is in a passive position, because the wind pressure affects the plates 6 from the rear and moves them to the vane position (Leiren, 2020; Uzakov, 2023). It can be seen from the figure that the asset.

2 MATERIALS AND RESEARCH METHODS

It can be seen from the figure that the center of the active wing 3 has a width of open surface 7 that passes

[a] https://orcid.org/0009-0000-4567-7734
[b] https://orcid.org/0009-0000-7951-2110
[c] https://orcid.org/0009-0009-4776-1820
[d] https://orcid.org/0009-0002-6037-3768

the wind flow. The wings are interconnected by steel ropes 8 at the lower and upper ends of the wings. This allows the wing to operate without jerks in the instantaneously changing wind speed, it isolates the wings (Saidur, 2011; Mamatkulova, 2024).

This process, which happened around the shaft 1 of the lower tier, takes place in the second tier of the rotor around the shaft 9, with only the opposite movement.

If we put the second layer of the rotor on top of the first layer of the rotor, the rotor shown in Figure 3a is formed.

In this case, the assembly process is as follows: the shaft 9 is passed through the shaft 1, and with the help of links with a joint (radial bearing), the upper and lower tiers of the rotor are ensured to rotate in opposite directions (Fig. 3b). The vertical position of the shafts is ensured as follows: the shaft 9 is mounted on the radial-support bearing 10 in the lower part, and the shaft 1 forms a hinged joint with the help of the radial bearings 11 and 12.

In turn, the shaft 1 is fixed to the frame 13 with the help of radial bearing 14 and support bearing 15.

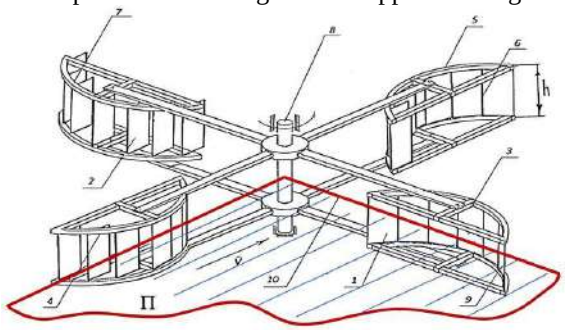

Figure 1: A single-stage rotor with an open center of the blade.

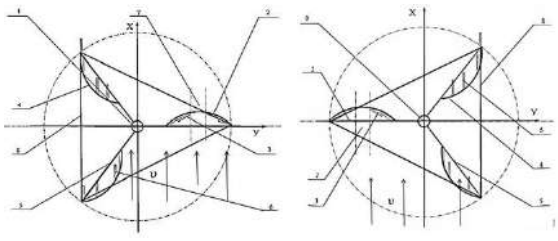

a) b)

Figure 2: Horizontal of the two layers of the rotor.

Another important aspect of the design is that the center of each wing is left open to let the wind flow through (Figure 4). If we pay attention to the figures, we can estimate that the aerodynamic processes of the wind flow are different in rotor constructions with a wing consisting of a central open part of the working surface 7 and a wing with a fully closed working surface (Olabi, 2021; Kudelin, 2021).

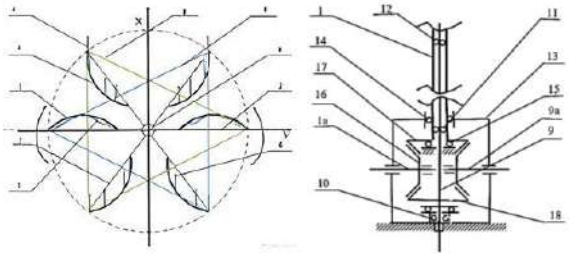

a) b)

Figure 3: 3-assembled view of the rotor.

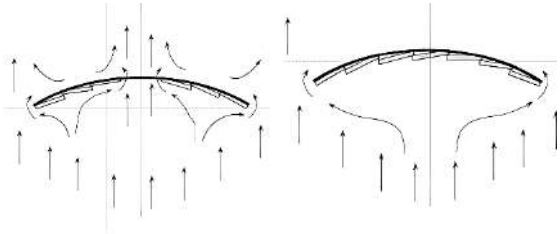

a) b)

Figure 4: a) open and b) closed surface wings.

In the following, we define the mathematical expression of the driving moment for the rotor design

It is known that the rotor may operate in four distinct positions, each associated with a corresponding change in the driving force applied to the wings during one cycle of operation. In this paper, we will analyze the second and third positions and derive their respective expressions.

An active cathode with the center plate relay open. According to it, the wind flow enters along the concave surface of the wing and flows along the central zone. While the central opening helps to suck the static air behind the wing in its direction, the wind stream flowing through the peripheral zones sucks the trailing static air close to it. In this way, the value of the air mass flowing over the wing surface increases (Hannan, 2023; Uzakov, 2023).

3 RESULTS AND DISCUSSIONS

The aerodynamic process on the surface of the rotor with the central plate open can be analyzed as follows: according to Bernoulli's equation.

$$p_1 + \frac{\rho \cdot \vartheta^2}{2} + z_1 \cdot \rho \cdot g = p_2 + \frac{\rho \cdot \vartheta_2^2}{2} + z_2 \cdot \rho \cdot g \quad (3)$$

Here, p_1 and p_2 are the static pressure on the surfaces, $\vartheta_2^2/2$ is the aerodynamic pressure, and z is the height of the surfaces through which the wind flows. Since in our conditions the wind current flows over a surface of uniform height, we can write equation (1) as follows:

$$p_1 + \frac{\rho \cdot \vartheta_1^2}{2} = p_2 + \frac{\rho \cdot \vartheta_2^2}{2} \quad (1)$$

Therefore, the pressure difference, which is the main indicator of energy production, will be equal to equation (3).

$$p_1 - p_2 = \frac{\rho \cdot \vartheta_1^2}{2} - \frac{\rho \cdot \vartheta_2^2}{2} \quad (2)$$

The essence of this equation is that in the zone of increased kinetic pressure, the static pressure decreases, and vice versa, the static pressure increases. Due to the almost motionless air behind the wing, the static pressure increases, and it tends to the areas of the wing that pass the wind flow, creating a relative vacuum behind the wing - that is, this process leads to the equation of non-self (continuity of the environment) of the flow ($S_1\vartheta_1 = S_2\vartheta_2$) according to the fact that the wind speed in the open part of the center of the wing increases slightly (Westerlund, 2020).

Based on the above-mentioned scientific research and certain technical laws, the proposed new design of the rotor of the wind turbine is shown in Figure 5.

The second position occurs when the second wing is restricted from moving in the direction of the wind at point B of the first wing, in shape 1. The third position is when the second wing travels from point A of the first wing relative to the direction of the wind, in shape 2.

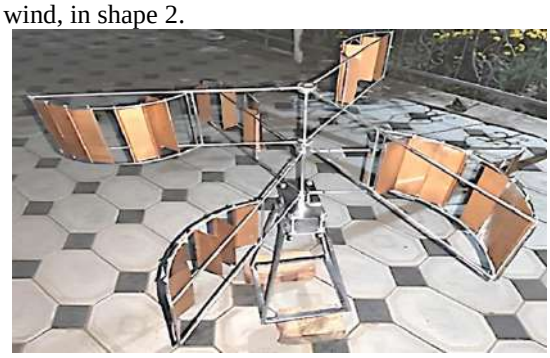

Figure 5: Rotor of wind turbine "Samarkand", № IAP 2022 0106.

The thrust moment they are generated by the rotor when in position 2 is influenced by the angle at which the wings are oriented relative to the oncoming wind. This angle significantly impacts the thrust generated, which is determined by how the operating surface of the second wing varies. The first wing is always fully operational. This is the statement of the second wing:

$$l \cdot \sin\varphi = r \cdot \sin(180 + \delta_1) \quad (4)$$

Equality begins with finding a solution. Precisely,

$$\delta_1 = \arcsin(-\frac{l}{r}\sin\varphi) \quad (5)$$

when equals the value, the angle of inclination of the first wing in the starting position begins with angles at the corners of the first and second wings. As a result, the forming surface of the second wing at a α_{s4} angle generates no driving torque. In this case, α_{s4} increases as φ increases, and its value can reach 90 degrees. Consequently, it is completely blocked by the second wing. In Form 1, α_{s4} represents an angle. The challenge lies in determining how α_{s4} varies when the angle of inclination changes.

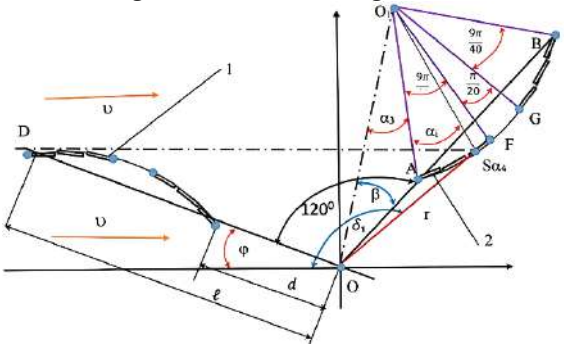

Figure 6: Regarding the calculation of the torque of the Rotor 2nd wing in position 2.

Occurs when the value is. When the values of the φ and φ +1200 angles on the second wing increase, the angle of inclination of the first wing at the initial position begins to move toward the second wing. As a result, the surface formed at the base of the corners of the second wing doesn't create driving torque. In this case, the α_{s4} angles increase by φ and their value reaches 90^0. This is fully covered by the second wing when in form 1. In form 1, the α_i angles are represented as number α_{s4}, where the question of determining the change in value from φ to α_{s4} when the angle moves from answered.

From the drawing

$$\frac{R}{\sin(\angle O_1OS_{\alpha 4})} = \frac{R}{\sin(\angle O_1OA + \angle AO_1OS_{\alpha 4})} = \frac{R}{\sin(\angle OO_1S_{\alpha 4})} \text{ or}$$

$$\frac{R}{\sin(\beta + \delta_1 - (\varphi + \frac{2\pi}{3}))} = \frac{r}{\sin(\alpha_3 + \alpha_{s4})} \text{ and in this } \delta_1 = \delta + \frac{2\pi}{3}$$

considering that $\sin(\alpha_3 + \alpha_{s4}) = \frac{r}{R}\sin(\alpha + \beta - \varphi)$

and and from it we find the final equation:

$$\alpha_{s4} = \arcsin(\frac{r}{R}\sin(\alpha+\beta-\varphi)) - \alpha_3$$

It is known that the expressions r, α_3, δ and β are represented by the following equations:

$$r = \sqrt{R^2 + |OO_1|^2 - 2|OO_1| \cdot \cos[\alpha + \alpha_3]}$$

$$\alpha_3 = \arccos\left(\frac{|O_1O|^2 + R^2 - d^2}{2 \cdot R \cdot |O_1O|}\right)$$

$$\delta = 2 \cdot arctg \frac{-B1 \pm \sqrt{B1^2 - 4A1 \cdot C1}}{2A1} \quad (6)$$

$$\beta = arctg \frac{|O_1C|}{l \cdot k + a}$$

To this equation and Fig balanid 2-wing for holding events based on the conditions of:

$0 \le \alpha_{s4} \le \alpha_F$

$$M_2 = \frac{1}{2} \cdot c \cdot \rho \cdot h \cdot \left[\left(\int_{\alpha_{s4}}^{\frac{9\cdot\pi}{40}} (\vartheta \cdot \sin\delta_1 - \omega \cdot r)^2\right) \cdot r \cdot d\alpha + \left(\int_{\frac{11\pi}{40}}^{\frac{\pi}{2}} (\vartheta \cdot \sin\delta_1 - \omega \cdot r)^2\right) \cdot r \cdot d\alpha\right]$$

$\alpha_F < \alpha_{S4} < \alpha_G$

$$M_2 = \frac{1}{2} \cdot c \cdot \rho \cdot h \cdot \left[\left(\int_{\frac{11\pi}{40}}^{\frac{\pi}{2}} (\vartheta \cdot \sin\delta_1 - \omega \cdot r)^2\right) \cdot r \cdot d\alpha\right] \quad (7)$$

$\alpha_G \le \alpha_{S4} \le \alpha_B$

$$M_2 = \frac{1}{2} \cdot c \cdot \rho \cdot h \cdot \left[\left(\int_{\alpha_{s4}}^{\frac{\pi}{2}} (\vartheta \cdot \sin\delta_1 - \omega \cdot r)^2\right) \cdot r \cdot d\alpha\right]$$

Here are the values derived from rotor design α_F, α_G and α_B: Based on the number of equations, it can be concluded that the second-stage wing undergoes three homogeneous dynamic transformations during its second position.

Once the tier 2 fan advances behind wing 1, modification φ transfers it to position 3. At the same moment, wing 2 begins to expand again in the direction of the wind from point A, which is its bottom section.

$d \cdot \sin\varphi \ge r \cdot \sin(180^0 - \delta_1)$ marks the start of state 3 of the limitations. Even in this instance, it will seem homogenous with the following equation:

$$\alpha_{S5} = \alpha_3 - \arcsin(\frac{r}{R}\sin(\alpha+\beta-\varphi)) \quad (8)$$

The arc-shaped surface formed on the angular base α_{s5} enters an active functioning state, whereas the surface built on the angular basis α_{s4} remains passive. This is critical for determining the limit of the integral.

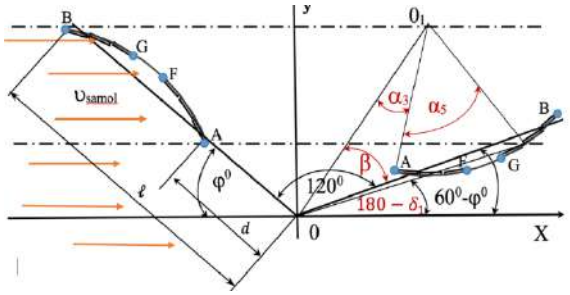

Figure 7: We calculate the torque of rotor wing 2 in position 3 using the following conditions.

$(\vartheta = \vartheta_{wind} - \vartheta_{werter}\ ;\ \alpha_{s5} = \alpha_5)$

$0 \le \alpha_{S5} \le \alpha_F,\quad \alpha_F \le \alpha_{S5} \le \alpha_G$ in the past

$$M_2 = \frac{1}{2} \cdot c \cdot \rho \cdot h \cdot \left[\left(\int_0^{\alpha_{S5}} (\vartheta \cdot \sin\delta_1 - \omega \cdot r)^2\right) \cdot r \cdot d\alpha\right] \quad (9)$$

And in the range, $\alpha_G \le \alpha_{S5} \le \alpha_B$

$$M_2 = \frac{1}{2} \cdot c \cdot \rho \cdot h \cdot \left[\left(\int_{\alpha_G}^{\alpha_{S5}} (\vartheta \cdot \sin\delta_1 - \omega \cdot r)^2\right) \cdot r \cdot d\alpha\right]$$

The equations will be suitable. It is worth noting that in scenario 2, angle α_{s5} will represent the integral's beginning coordinate, α_{s5} as well as its end coordinate. However, in the $\alpha_G \le \alpha_{S5} \le \alpha_B$ range, the surface moment caused by the wing autofocus arc will be relatively tiny, because the surface is nearly parallel to the wind direction.

The result is that the second wing undergoes two homogenous dynamic changes at the third position of the tier. The term "tier" indicates that the rotor is divided into two tiers. We studied the second wing of one tier here. The second wing of the second tier will have the same characteristics, but with a 60^0 delay.

These equations do not require answers in engineering calculations; instead, they allow you to calculate with the required precision utilizing computer-based approximate solution methods.

4 CONCLUSIONS

This study presents a novel two-tier rotor design for vertical-axis wind turbines, aiming to enhance aerodynamic efficiency and power generation in regions with variable wind conditions. By examining the dynamic interactions between airflows and rotor components, we established that the proposed rotor structure offers substantial improvements in torque production and airflow regulation.

The primary innovation lies in the division of the rotor into two symmetrical tiers, rotating in opposite directions. This configuration optimizes the use of wind energy by maximizing the relative velocity between the air and the rotor surfaces. The inclusion of an open-center design in each rotor blade significantly contributes to aerodynamic performance. This opening enables the evacuation of static air behind the wing, increasing the suction effect and reducing drag, thereby facilitating more effective conversion of kinetic wind energy into mechanical energy.

From the experimental and theoretical modeling, it was observed that the aerodynamic drag coefficient of the rotor reaches up to 1.4, which indicates a high capacity for energy extraction. Furthermore, the two-tier system provides operational stability regardless of wind direction changes. The rotor adapts to these variations without requiring additional orientation mechanisms, which simplifies its construction and reduces maintenance requirements.

Mathematical modeling based on Bernoulli's principle and torque equations revealed that the second-tier blades undergo two or more distinct dynamic transitions during one rotation cycle, each contributing uniquely to torque production. These transformations depend on the angular displacement and wind interaction angle, highlighting the rotor's capability to self-regulate its aerodynamic load.

Importantly, the design simulates the energy yield of a six-blade rotor while maintaining the mechanical simplicity and efficiency typical of a three-blade system. This balance between complexity and output makes it highly suitable for decentralized energy production, especially in developing regions with modest technological infrastructure.

Finally, this research demonstrates that careful integration of aerodynamic theory, rotor geometry, and innovative design features can yield a wind turbine rotor capable of delivering stable, efficient, and high-performance energy generation. The findings contribute to the ongoing advancement of sustainable wind technologies and present a promising solution for enhancing wind energy capture in various environmental conditions.

ACKNOWLEDGEMENTS

This investigation provided on the base of budget funding of the Uzbekistan Academy of Sciences.

REFERENCES

Manwell, J.F., McGowan, J.G., Rogers, A.L., 2009. *Wind Energy Explained*, Wiley.

Zhang, Z., Liu, X., Chen, J., 2023. *Overview of the development and application of wind energy in New Zealand.* Energy and Built Environment.

Chaurasiya, P. K., Warudkar, V., Ahmed, S., 2019. *Wind energy development and policy in India: A review.* Energy Strategy Reviews.

Jain, P., 2010. *Wind Energy Engineering* J. Exp. Psychol. Gen.

Dekhkanov, U., Tillaboev, Y., 2024.*The equation of the driving torque generated by the concave surface rotor blade under the influence of wind pressure*. AIP Conf. Proc. 3004, 060003.

Leiren, M. D., Aakre, S., Krug, M., 2020. *Community acceptance of wind energy developments: Experience from wind energy scarce regions in Europe.* Sustainability (Switzerland).

Uzakov, G.N. et al., 2023. *Modeling of heat exchange processes in a condenser of a pyrolysis bioenergy plant*. In BIO Web of Conferences (Vol. 71, p. 02021). EDP Sciences.

Saidur, R., Rahim, N. A., Solangi, K. H., 2011. *Environmental impact of wind energy.* Renewable and Sustainable Energy Reviews.

Mamatkulova, S. G., et al, 2024, "*Modeling and Analysis of the Kinetics of the Pyrolysis Process of Biomass with Influence Raw Material Composition on Comsol Multiphysics*," International Conference on Technological Advancements in Computational Sciences (ICTACS).

Olabi, A. G., Wilberforce, T., Abdelkareem, M. A., 2021. *Selection guidelines for wind energy technologies.* Energies.

Kudelin, A., Kutcherov, V., 2021. *Wind ENERGY in Russia: The current state and development trends.* Energy Strategy Reviews.

Hannan, M. A., Al-Shetwi, A. Q., Mahlia, T. M., 2023. *Wind Energy Conversions, Controls, and Applications: A Review for Sustainable Technologies and Directions.* Sustainability (Switzerland).

Uzakov, G. et al, 2023. Simulation of a tubular pyrolysis reactor using comsol multiphysics software. Cham: Springer Nature Switzerland.

Westerlund, M., 2020. *Social acceptance of wind energy in urban landscapes.* Technology Innovation Management Review.